hydrology

MDPI

Article

Evaporation from Porous Rock: Deciphering the Importance of Measuring the Evaporation Front Depth

Martin Slavík * and Martin Lanzendörfer

Faculty of Science, Charles University, Albertov 6, 128 00 Prague, Czech Republic; martin.lanzendorfer@natur.cuni.cz
* Correspondence: martin.slavik@natur.cuni.cz

Abstract: The study is concerned with the rate of evaporation from porous rock, including the second stage of evaporation characterised by the existence of a dry surface layer separated from the wet capillary zone by a sharp evaporation front. The main objective is to investigate the relationship between the depth of evaporation front and the rate of evaporation as the drying process progresses, and to compare measured evaporation rate with the corresponding calculated values. Sandstone core samples saturated with water were allowed to dry naturally under room conditions, while the changes in the evaporation rate and the depth of evaporation front, among other quantities, were measured. We demonstrate that the evaporation rate can be very accurately determined from the depth of the evaporation front and the ambient air temperature and relative humidity using Fick's law for water-vapor diffusion. During the second stage of evaporation, the diffusion flux through the dry surface layer is computed using the water-vapor diffusion coefficient of the rock, determined from a separate wet cup experiment. In order to cover the first stage of evaporation, an additional parameter characterising the diffusion layer of air above the surface is required, either determined by the best fit to the measured evaporation rates, or adopted from previous studies. The calculated evaporation rate was in good agreement with measurements, with Pearson correlation coefficient 0.98 and relative error of the calculations averaging 15% over the evaporation front depths ranging from 0 to 29 mm. A workflow for determining the evaporation rate from sandstone outcrops is suggested, along with possible applications in sandstone weathering research.

Keywords: evaporation; sandstone; uranine-probe; evaporation front; vaporization plane; weathering; salt weathering; diffusion

check for updates

Citation: Slavík, M.; Lanzendörfer, M. Evaporation from Porous Rock: Deciphering the Importance of Measuring the Evaporation Front Depth. *Hydrology* **2024**, *11*, 133. https://doi.org/10.3390/hydrology11090133

Academic Editor: Ezio Todini

Received: 12 June 2024
Revised: 19 August 2024
Accepted: 20 August 2024
Published: 23 August 2024

1. Introduction

Evaporation plays an important role in many natural processes. It is a key member of a water balance, being a major consideration in the design and management of water supply reservoirs. The evaporation from porous materials is an intriguing and intensively studied topic in natural and engineering sciences encompassing hydrology, agriculture, and soil sciences. Its critical role in rock weathering deserves particular attention. Evaporation affects the moisture content within the rock, its temporal changes, and spatial distribution, all of which influence the intensity of frost weathering [1–3]. Along with other factors (nature of salts, their resulting spatial distribution in the pore space, durability of the rock), the rate of evaporation influences the intensity of salt weathering [4,5] via the amount of salts crystallized. As a result, the areas with the highest evaporative loss coincide with the most intense rock weathering, as the majority of salt crystallisation occurs in these evaporation zones [6], leading to development of various weathering forms [7]. Cyclical changes in moisture content due to evaporation can also contribute to rock disintegration by causing variations in volumetric changes due to hygric or hydric dilatation [8,9]. Therefore, to make at least a rough estimate of the evaporation rate should be considered as one of the essential parts of rock weathering research.

The rate of evaporation from porous materials, as evidenced from soil evaporation studies [10], depends on the moisture characteristics of the material. When the liquid water in the pores is hydraulically connected to the surface of the material via a network of capillaries, the evaporation rate is relatively high, governed by the evaporative demand at the surface. This phase is called stage 1 of evaporation [11,12]. As the material dries, a dry zone develops within the material near the surface, and the evaporation rate is then controlled by diffusion [10]. This phase of considerably lower evaporation rate is commonly referred to as stage 2 of evaporation. It has been discussed in [13] that the formation of the dry zone, marking the transition from the first to the second stage, depends mainly on the width of the pore size distribution.

In contrast to soils, the process of evaporation from rocks is less well described in the literature. We can mention the now classic studies on evaporation from bricks and building materials [14,15], or the laboratory studies [16,17] which focused on monitoring several parameters during evaporation from sandstone. Several recent works [7,18–20] have considered the spatial distribution of moisture in determining the rate of evaporation from porous rocks. The evaporation rate in these studies was not only measured, but also calculated using Fick's law of diffusion. Only four parameters were used in the calculation: air temperature, air humidity, water-vapor permeability of the rock and depth of the evaporation front. The first two can be easily obtained using standard equipment, while the water-vapor permeability can be measured in the laboratory.

The evaporation front is a relatively recent concept in rock weathering research [5,7]. It refers to an apparently sharp interface in the rock outcrop, demarking the zone of distinct liquid capillary water from the much drier zone near the surface [21–23]. During the evaporation process, liquid water is brought from the greater depth to the evaporation front through the capillary zone, as can be mathematically described by the Richards equation [24]. In the dry surface layer on the other side, the connectivity of the capillaries is diminished, and the moisture is transported predominantly in the form of water vapor by diffusion. The position of the evaporation front, and its eventual movement, is the result of two opposing processes: the loss of moisture by evaporation and the influx of moisture from the rock [23]. If the rate of evaporation exceeds the rate of inflow, the evaporation front moves deeper below the surface, and vice versa. Importantly, in both cases the evaporation rate is limited by the rate of vapor diffusion through the dry surface layer and is thus effectively governed by the actual depth of the evaporation front.

The applicability of the evaporation front concept to determine the evaporation rate in the rock was supported by both laboratory and field measurements, and a novel microdestructive method called uranine-probe has recently been developed, which uses a moisture-sensitive dye to detect the depth of the front with high accuracy [22]. The evaporation front was found to be positioned from the very surface up to decimeters below the rock surfaces [22,25,26], a range that alters the evaporation rate over several orders of magnitude by theory, the diffusive flux being inverse proportional to the front depth by the Fick's law [27]. It was suggested in [19] that the position of the evaporation front is a primary factor controlling the evaporation rate from natural rock outcrops in various climates, including arid, semi-arid, and humid environments. This highlights the need to know the depth of the evaporation front when determining the evaporation rate from rock outcrops.

In previous studies, the evaporation rate values calculated using the known evaporation front depth were in good agreement with the measurements, but these studies were limited to a static evaporation front that was artificially fixed at a certain constant depth throughout the experiments. To our knowledge, only a few [16,17,23] evaporation experiments have documented the progression of the moisture distribution within rock from complete saturation to complete drying, cf. [10] for soils. The present study aims to provide the first evidence that the concept of combining the knowledge of the natural evaporation front depth with Fick's law makes a reliable assessment of the evaporation rate possible. This may allow for a quantification of moisture fluxes and hence the water balance in natural rock outcrops, which are important parameters in field studies of all moisture-affected weathering processes.

Our study specifically deals with sandstone because it is one of the rocks most affected by weathering. The primary objective is to investigate the relationship between the depth of the evaporation front and the rate of evaporation as the drying process progresses. We compare the directly measured evaporation rates with those calculated using the combination of Fick's law and the uranine-probe method. We discuss the accuracy of the prediction, the relationship with the water content and the pore size distribution, the methodology for determining the evaporation rate from sandstone outcrops and finally, the implications for sandstone weathering research.

2. Materials and Methods

The experimental setup was designed as follows. The originally fully saturated sandstone samples were allowed to evaporate under room conditions and the rate of evaporation was obtained by weighing the samples. At the same time, the evolution of the depth of the evaporation front below the surface of the samples was determined. The relative surface moisture of the sandstone was also measured. The measurements were accompanied by air humidity and air temperature recording. Material properties were determined in the laboratory. The evaporation rate was calculated using Fick's law and then compared with the measurements.

2.1. Rock Used

We used a medium- to fine-grained Turonian quartz sandstone (*JE sandstone*, as labeled after the municipality of Jestřebice) of the Bohemian Cretaceous Basin (Czech Republic, Figure 1). The sandstone was sampled from the boulders of a collapsed sandstone pillar using a hand-held drill with a diamond core bit. The samples were initially in the form of a core 8 cm in diameter and ~4 cm thick, which was later slightly modified in size (see below).

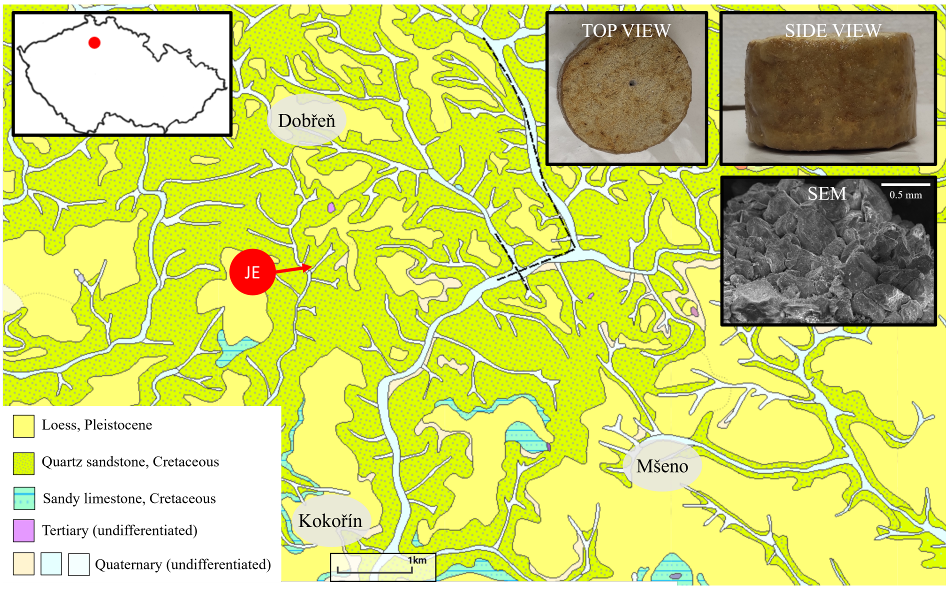

Figure 1. Geological map [28] of the area where the JE sandstone samples were taken (sampling location shown by the red dot and arrow). Top right is a photograph of the samples sealed in epoxy and below is a scanning electron microscope image of the pore space of the JE sandstone.

The fundamental characteristics of porous materials that affect moisture flow and its spatial distribution include total porosity and pore size distribution. To determine these characteristics for the JE sandstone, we used two methods: (i) a conventional high-pressure mercury intrusion porosimetry (MIP, see [29]) using an AutoPore IV 9520 instrument (Micromeritics); and (ii) a series of saturated flow experiments with non-Newtonian fluids following the methodology by Abou Najm and Atallah [30], called ANA method in the remaining text. In contrast to MIP, the ANA method provides an approximated functional pore size distribution of the porous media, defined by the equivalent idealized representation of the saturated flow by bundles of parallel capillaries, see Appendix A.

The intensity of the water-vapor flow in stage 2 of evaporation depends on the water-vapor permeability of the rock. In this study, we determined the water-vapor diffusion coefficient δ (s) of the JE sandstone using the following method adapted from EN ISO 12572:2001, as described by [19]. The rock cores were reduced in size to fit into PVC tubes 75 mm in diameter. The cores were then placed in the tubes and sealed with epoxy to prevent water-vapor escape between the sandstone core and the tube wall. Another PVC tube, partially filled with deionized water, was attached end-to-end to the first tube, and sealed with electrical tape to limit water-vapor loss from the setup to less than 0.4 g per week [31]. The deionised water maintained a relative humidity (RH) of 100% below the core but did not come into direct contact with the core. This arrangement, referred to as a *wet cup*, is illustrated in Figure 2A.

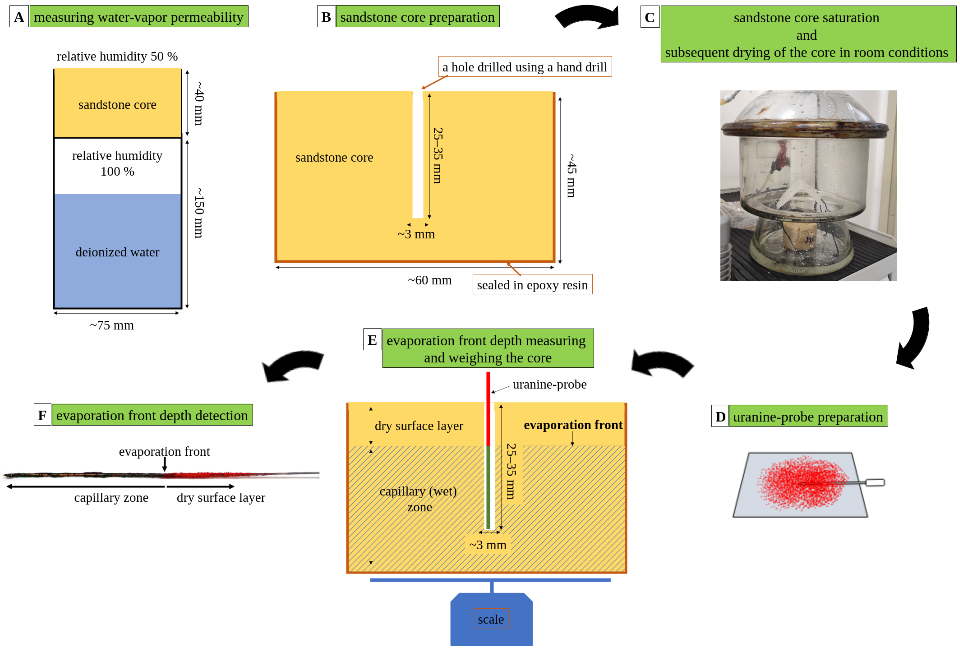

Figure 2. Workflow of the measurements made during the evaporation experiment. (**A**) Scheme of the measurement of the water-vapor diffusion coefficient in wet cups. (**B**–**F**) Successive steps in the measurement of the evaporation rate and the evaporation front depth. Parts (**D**,**F**) adapted from [22].

Three wet cups were placed in a CTC 256 Memmert climatic test chamber (Memmert, Germany) with 50% RH and a temperature $T = 20\,^\circ\mathrm{C}$, which was homogenized by a fan. The water vapor diffused through the sandstone core due to the water-vapor pressure gradient, causing weight loss in the wet cup. The weight was recorded periodically, determining the water-vapor mass flux j (kg/(m^{2}s)) for each time interval Δt (s) between the measurements:

$$j = \frac{\Delta m}{S \Delta t}, \tag{1}$$

where Δm is the mass decrease (kg) over the time interval and S is the evaporating surface area (m^2). (Note that j is related to the evaporation rate E (m/s) through $j = \rho_w E$, denoting by ρ_w the density of liquid water.) The water-vapor diffusion coefficient δ (s) was then calculated from Fick's law of diffusion:

$$j = \delta \frac{\Delta p}{d}, \tag{2}$$

where d is the sample thickness (m) and Δp is the difference in partial water-vapor pressure within the core (Pa). Note that δ is related to the traditional mass diffusivity D through $\delta/D = RT/M_{\mathrm{H_2O}} \doteq 1.35 \times 10^5\,\mathrm{m^2/s^2}$ at room temperature. The partial water-vapor pressure was calculated from the recorded values of ambient temperature T (°C) and relative humidity RH values by the classical Tetens formula [32] (cf. [33]):

$$p = \frac{RH}{100}\,610.78\exp\left(\frac{17.27T}{T+237.3}\right). \tag{3}$$

The weight change was monitored for 28 days and checked for linearity. It's worth noting that the wet cups were not employed for the subsequent evaporation rate measurements (as described below).

2.2. Evaporation Rate Measurements

Three JE sandstone cores were used for the evaporation rate measurements. The surface of the cores, except for the upper base, was coated with epoxy. The cores were modified by drilling a hole with a 2 mm drill from the top base to approximately three quarters of the core thickness for evaporation front depth measurements. The evaporating surface area of the cores was 26.6 to 29.9 $\mathrm{cm^2}$ and the thickness of the cores varied from 3.9 to 5.6 cm (Figure 2).

The sandstone cores were saturated with water and then allowed to dry out through their upper base only under room conditions (with $T{\sim}17$ °C and RH∼42%). As the cores dried, their weight was recorded using a balance (P221, LESAK, resolution 0.1 g) and the depth of the evaporation front was measured. In the early phase of the experiment, when the evaporation rate was high, measurements were made at least three times a day. As the experiment progressed and the evaporation rate decreased to <0.3 mm/day, the measurement frequency was reduced to at least twice a day.

The uranine-probe method described in [22] was used to measure the depth of the evaporation front. A stainless steel medical needle coated with red water-soluble uranine powder (CAS number 518–47-8) was inserted into the drilled hole. After 5–10 min, the depth of the boundary between the red and dark-orange to green part of the needle was measured to determine the depth of the evaporation front with an accuracy of ±2 mm (Figure 2, [22]). Between measurements, the hole was plugged with an approximately 3 mm long plug made of a binding wire wrapped with Teflon tape. Framework of the workflow is illustrated in Figure 2.

The evaporating surface area of the cores was determined by measuring it on millimeter paper. The weight change in grams per day was then converted to the evaporation rate in millimeters per day using the area of the evaporating surface and the density of water. The measurements of the evaporation rate were accompanied by the measurements of RH and T of the air at 1-min intervals by a Voltcraft DL-121TH (*RH + T sensor* further) located ∼20 cm above the cores. The accuracy of the device is ±3% (RH) and ±1 °C (T). The RH and T logs were used in subsequent calculations (see below). In addition, the surface relative moisture of the cores was measured using a Protimeter GMR 110 (Greisinger), which provides reference values of electrical resistivity (*surface moisture* further).

2.3. Evaporation Rate Calculations

During stage 1 of evaporation, the capillary (wet) zone reaches the very surface of the porous material. With the depth of the evaporation front being effectively zero, the evaporation rate is not hindered by the water-vapor diffusion within the rock, but it is only limited by the vapor transport through a thin layer of air above the rock surface. As long as the actual evaporation rate does not reach the potential evaporation, the corresponding mass flux j (similarly to the previous section) meets the Fick's law of diffusion $j = C\Delta p$, representing a layer of unspecified thickness and diffusive coefficient. For a convenient correspondence with the later description of stage 2 evaporation, the parameter β has been introduced [19] by the formula

$$j = \delta \frac{\Delta p}{\beta}. \tag{4}$$

Knowing the rock's water-vapor diffusion coefficient δ, the parameter β can be determined by the least squares fit that minimizes the difference between the measured evaporation rate and the rate calculated using (4). Conceptually, the factor δ/β represents the boundary layer of variably water-vapor saturated air created over an evaporating surface [34] which limits the water-vapor flux from the evaporating surface further into the atmosphere, thereby reducing the rate of evaporation. Note that the layer properties are influenced by additional conditions such as local air movement and local surface geometry; here it is represented as a virtual extension of the rock with its diffusion coefficient δ up to the distance β from the actual rock surface. The parameter β should not be confused with the thickness of a layer of air with elevated humidity near the surface, which may be different. The parameter β has been shown to be a practical way to estimate the evaporation rate when considering the evaporation front at the surface in [18], where the value $\beta = 0.80$ mm was determined for the JE sandstone based on a one-year outdoor experiment.

The main focus of the present study is the stage 2 of evaporation, when the depth of the evaporation front is non-zero and the evaporation rate is limited by the dry surface layer. The evaporated mass flux j is then determined by the diffusion through the dry layer of the rock as follows,

$$j = \delta \frac{\Delta p}{L}. \tag{5}$$

Here the parameter L denotes the depth of the evaporation front (m) as measured by the uranine-probe method. The depth of the evaporation front changed during the individual observation periods. Therefore, in our calculations, we use the arithmetic mean of the depth of the evaporation front at the beginning and end of each observation period.

The actual evaporation rate is constrained by the smallest of the diffusive fluxes considered above. Thus, while (4) governs the evaporation rate in stage 1, (5) is only valid as soon as L is greater than β. For simplicity, we computed the evaporation rate during the entire experiment, including the very first part of stage 2, by the united form

$$j = \delta \frac{\Delta p}{\min(L, \beta)}. \tag{6}$$

Same as in Section 2.1, in Equations (4)–(6), Δp is the difference in partial water-vapor pressure between the evaporating surface and the evaporation front. The partial water-vapor pressure was calculated from the values of temperature T and relative humidity RH using (3). For the evaporating surface of the rock, T and RH values from RH + T sensors were substituted. For the evaporation front, T values from RH + T sensors were used, and the constant RH = 100% was substituted, assuming fully saturated water-vapor at the evaporation front. This corresponds to the assumption that the evaporation rate is controlled solely by the flux due to vapor diffusion through the surface layer. Lower RH values at the evaporation front should be considered for suction pressures exceeding 2–3 MPa ([35], see also Section 4.2) or in the presence of salts (see Section 4.5), none of that being assumed here.

3. Results

The results section is structured as follows. First, the characteristics of the studied rock are presented, then the measured values of the evaporation rate, the depth of the evaporation front, and the surface moisture during the evaporation experiment are given. The calculated values of the evaporation rate are then provided, and they are compared with the measurements.

3.1. Sandstone Characteristics

The total porosity of the JE sandstone was 0.29 according to mercury intrusion porosimetry, the porosity measured by comparing the weights of the saturated and dry sample was 0.283 for the sample measured by the ANA method. The pore size distribution of JE sandstone determined using the mercury intrusion porosimetry is presented in Figure 3a. The functional PSD approximation of JE sandstone obtained using the ANA method is presented in Table 1 and Figure 3b. The experimental data used in the ANA method (the material parameters of the non-Newtonian fluids and the corresponding volumetric fluxes observed by the saturated flow experiments) are summarized in Appendix A, Table A1. Both the mercury intrusion porosimetry and the ANA method show the pore radius of the peak in the volumetric pore size distribution at 28 μm and 27 μm, respectively. The MIP indicates a rather narrow pore size distribution, where 95% of the pore volumes are larger than 4.5 μm and 99% are smaller than 48 μm. The functional PSD approximation is also consistent with a narrow distribution, as shown in Figure 3.

Table 1. Functional pore size distribution approximation by ANA method.

R_j (μm) **Pore Radii (Given)**	w_j (–) **Relative Fluxes for Water**	$\mathrm{vol}(R_j)\, w_j$ (–) **Pore Volumes**
10.0	0.001	0.003
13.9	0.001	0.001
19.3	0.001	0.001
26.8	0.485	0.180
37.3	0.508	0.098
51.8	0.001	0.000
72.0	0.001	0.000
100	0.001	0.000

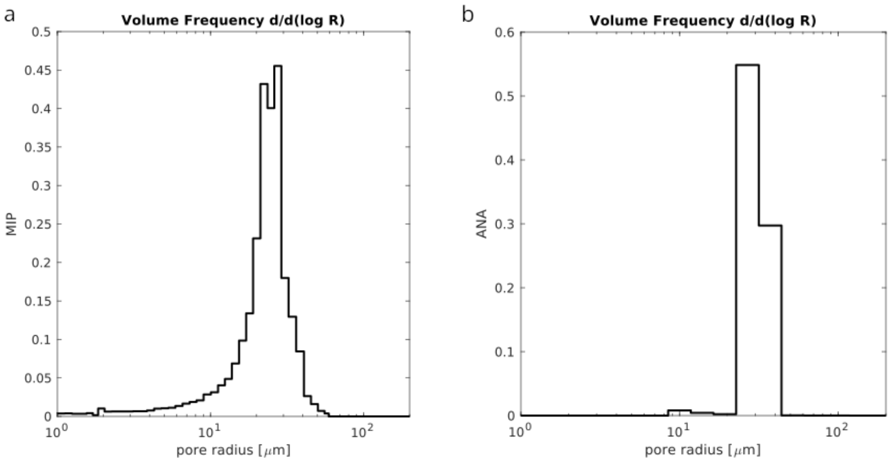

Figure 3. (**a**) PSD measured by MIP. (**b**) Functional PSD computed by ANA.

The water-vapor diffusion coefficient δ of the JE sandstone varied from 3.07×10^{-11} to 3.17×10^{-11} s for the three wet cups. The average of these values, $\delta = 3.12 \times 10^{-11}$ s, is used to calculate the evaporation rate. This value is equivalent to mass diffusivity $D = 4.23 \times 10^{-6}\ \mathrm{m}^2/\mathrm{s}$ at room temperature.

3.2. Measured Values

During the 11.5-day campaign, a total of 32 individual measurement periods were observed, lasting from 4 to 15 h each. The weight of the samples was recorded to determine the evaporation rate, and the depth of the evaporation front was measured using the uranine-probe method. Surface moisture values were also monitored. The experiment was carried out on an average T of 17.4 °C (16.9–18.8 °C) and an average RH of 42.3% (38.4–44.8%).

Initially, the evaporation rate for all three samples ranged from 1.8 to 2.5 mm/day and remained stable for approximately 2 days. From the second to the fourth day, the evaporation rate increased slightly to 2.8, respectively 3.5 mm/day for individual samples, the highest rate recorded throughout the experiment. Approximately 4 days after the experiment started, the evaporation rate sharply declined. By the end of the experiment, the evaporation rate reached approximately 0.1–0.2 mm/day, which is only ∼3% of the highest value (Figure 4A). Note that the slight fluctuations in the evaporation rate in the second half of the experiment (from about day 7) are due to the resolution of the scale used to weigh the sandstone samples.

At the beginning of the experiment, the evaporation front was at the surface of the sandstone and remained there for about 3 days for all samples as measured by the uranine-probe. Then it moved below the surface, gradually retreating to a depth of 26–29 mm over the next 8 days (Figure 4B). Surface moisture values started at 25–26 REF and gradually decreased to 5–7 REF by the end of the experiment (Figure 4C).

In the following text, we refer to stage 1 when the evaporation front is measured to be on the sandstone surface and to stage 2 when a nonzero evaporation front depth is measured. Stage 1 persisted for approximately the first 3 days, characterized by a relatively high evaporation rate and maximum surface moisture values. The transition from stage 1 to stage 2 was followed by a sudden decrease in the evaporation rate (Figure 4A), and accompanied by a substantial decline in surface moisture levels (Figure 4C). Stage 2 was characterized by an increasing depth of the evaporation front, much lower and decreasing evaporation rates and lower and decreasing values of surface moisture. The thickness of Sample 1 (5.6 cm) was larger compared to the other two samples (4.1 and 3.9 cm), obliging the evaporation front depth to progress slower.

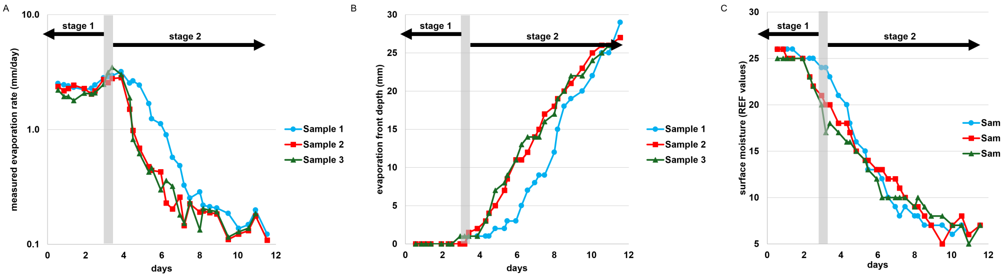

Figure 4. Evolution of (**A**) measured evaporation rate (vertical axis is logarithmic), (**B**) evaporation front depth, (**C**) surface moisture values during the experiment. The transition from stage 1 to stage 2 for all the samples is indicated by the grey area.

3.3. Calculated Values

The evaporation rate was calculated using the Fick's law embodied in (6) and the measured evaporation front depth substituted for L. The parameter β, characterizing the stage 1 of evaporation, was determined through an iterative least squares method to achieve the best possible fit between the measurements and the calculations for all three samples. The best-fit value, presented in further calculations, was determined as $\beta = 1.38$ mm. Alternatively, evaporation rates calculated using $\beta = 0.80$ mm (the value determined in [18], based on an outdoor experiment) are presented for comparison.

The evolution of the calculated evaporation rate aligns well with the measurements in general (Figure 5). Initially, the evaporation rate was relatively high (2.2 mm/day) and then even slightly increased (up to 2.4 mm/day) until the end of stage 1. Then, approximately 3.5–4 days after the start of the experiment, there was a sharp decrease in the evaporation rate as the evaporation front retreated below the surface, marking stage 2. Subsequently, the calculated evaporation rate gradually decreased to approximately 0.1–0.2 mm/day by the end of the experiment. The timing of the transition from higher to lower evaporation rates was consistent between the calculations and measurements (Figure 5). The average relative error (with respect to the measured values) was 15%, corresponding to the absolute difference of the calculated versus measured evaporation rates being 0.16 mm/day throughout the experiment (Table 2). In stage 1, the difference between calculations and measurements averaged to 0.21 mm/day for all samples (maximum difference was 0.50 mm/day), with an average relative error of 9%. In stage 2, the difference averaged 0.15 mm/day, with an average relative error of 17%.

Table 2. Average absolute difference and relative error between calculated and measured evaporation rates for the three samples, and for all samples together.

	Sample 1	**Sample 2**	**Sample 3**	**All Samples**
Average absolute difference (mm/day)				
for stage 1	0.23	0.17	0.23	0.21
for stage 2	0.16	0.15	0.14	0.15
for the entire experiment	0.18	0.13	0.19	0.16
Average relative error (%)				
for stage 1	9	7	12	9
for stage 2	14	17	20	17
for the entire experiment	13	14	18	15

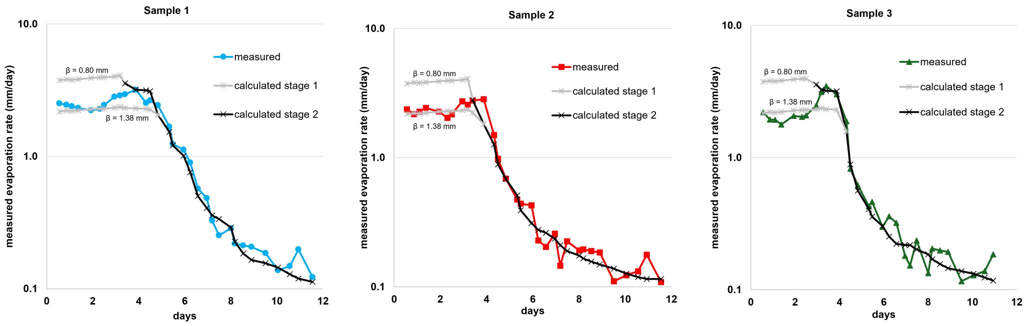

Figure 5. Comparison of evaporation rate calculations and measurements for individual samples. The grey curves show the calculated values for stage 1 if values of 0.80 mm and 1.38 mm are substituted for the parameter β. Note the logarithmic vertical axis.

4. Discussion

In this section, we begin by examining our findings within the context of the existing literature. Subsequently, we describe the relationship between the depth of the evaporation front and the corresponding evaporation rate. We also address potential uncertainties associated with the calculation of evaporation rates from natural sandstone surfaces. In addition, we present a workflow diagram, outlining the process for determining in situ evaporation rates. Lastly, we assess the implications of our results for research on sandstone weathering.

4.1. Relationship between the Evaporation Front Depth and the Evaporation Rate

A general view of the evaporation process from our sandstone samples is consistent with the knowledge gained from previous evaporation experiments conducted in soils [10]. At the beginning, with the liquid water reaching the surface, the evaporation took place at the surface, indicating stage 1. This was evidenced by the maximum surface moisture values as well as by the dissolution of the uranine-probe dye throughout the measured vertical profile, including the top surface of the sandstone. The rate of evaporation was relatively high because evaporation was not limited by the transport of liquid nor the water-vapor flow through the rock, but was only controlled by evaporative demand (this term usually pertains to all external factors such as air temperature, humidity, wind speed, solar radiation), resulting in high values of evaporation rate close to potential evaporation [36]. The observed variations in the evaporation rate within the first 4 days may be attributed to undiscerned changes in the evaporative demand or in the overlying boundary diffusion layer, as observed in previous studies [10,13].

The transition from stage 1 to stage 2 is attributed to the breakage of the capillary connections between the liquid water region and the surface [13]. Likewise, in our experiment, the interruption in hydraulic connectivity led to the retreat of the evaporation front below the sandstone surface, forming a dry surface layer. The uranine-probe confirmed this, as the dye was no longer dissolved near the surface of the sandstone, indicating that the liquid water region was located deeper below the surface. The increasing distance between the liquid water region and the sandstone surface resulted in lower measured surface moisture values.

Once the dry surface layer has formed and the evaporation front was below the surface, we can speak of stage 2 of evaporation [10,11]. Unlike stage 1, stage 2 was characterized by a gradual decrease in the evaporation rate to values close to the measurement error given by the scale used. This is consistent with the evaporation rate in stage 2 being controlled by water-vapor diffusion through the dry surface layer [37]. As the thickness of the dry surface layer gradually increased (as observed from the uranine-probe), the liquid water evaporated at greater depths. As a consequence, the water-vapor diffused over an increasing distance between the evaporation front and the sandstone surface, resulting in diminishing evaporation rates.

The measured data show a consistent inverse proportional relation between the evaporation front depth and the evaporation rate during stage 2, as depicted in Figure 6. Moreover, the relation is consistent with the Fick's law for diffusion over the distance given by the measured evaporation front depth with the water-vapor diffusion coefficient of the given rock, as determined a priori by the wet cup experiment.

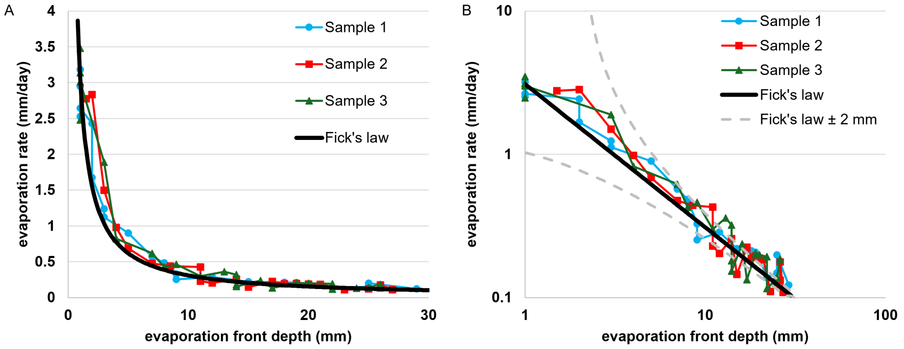

Figure 6. (**A**) Relationship between measured evaporation rate and measured evaporation front depth during stage 2 of evaporation. The theoretical relationship given by Fick's law is shown for comparison. (**B**) The same, expressed in log–log, with the effect on the calculated evaporation rate due to potential measurement errors ±2 mm of evaporation front depth (grey dashed lines).

4.2. Water Content and Evaporation Front Advancement

In general, the water content is unevenly distributed across the sample as well as across the wet capillary zone below the evaporation front in stage 2. Based on the observed total mass of water, we computed the average volumetric water content in the sample (the total volume of water divided by the volume of the sample) and similarly the average water content in the wet capillary zone (the total water volume divided by the sample volume excluding the dry surface layer above the evaporation front, as measured by the uranine-probe). The evolution of both values is presented in Figure 7. Assuming that the local water content is an increasing function of the depth, the latter average is guaranteed to be greater than the local water content near the evaporation front. While the nearly stagnating green line in Figure 7 for the first sample indicates that the evaporation front stabilized at the water content ∼0.04, the decreasing values particularly pronounced for the third sample demonstrate the contrary. However, that finding is in accordance with the theory, since the mass flux due to evaporation equals both the diffusive water-vapor flux in the dry zone and the liquid water flux in the wet capillary zone. Therefore, the lower the mass flux, the lower the hydraulic gradient and/or the unsaturated hydraulic conductivity in the vicinity of the evaporation front, which is consistent with the lower local water content (see also [23]).

For comparison, we calculated the "evaporation front yield" (dimensionless) defined here as the evaporation rate (mm/day) divided by the velocity of the evaporation front advancement (mm/day). In order to suppress oscillations and zero front velocities due to low resolution of the uranine-probe measurements, we took a moving average of the front depth over four successive measurements before computing the velocity. If the water content was uniform and constant across the capillary zone and the evaporation front was only descending along with its top layer being evaporated away, the "evaporation front yield" would be equal to the capillary zone water content (minus the residual water content in the dry surface layer, if any). The values presented in Figure 7 (black) are higher than the upper estimates of the water content. This is particularly notable during the first days of the experiment, where the plotted "yield" values exceed unity (in fact, they start from plus infinity in earlier days, due to zero evaporation front velocity), but it remains so throughout the experiment, as is again pronounced for the third sample. This is consistent with the decreasing average water content in the capillary layer; the faster the decrease in water content (the slope of the green line), the larger the "yield" with respect to the water content (the distance between the black and green lines). This further demonstrates that the entire capillary part of the sample is supplying the capillary water during the process, the evaporation front merely marking the location where the dominant liquid-water flux is replaced by the dominant water-vapor flux. The difference between the three samples was due to differences in their dimensions and, consequently, the total amount of water available for evaporation.

While the relation between the evaporation front depth and the evaporation rate is simple and robust, as described in Section 4.1, it is not sufficient for predicting the evolution of both quantities over time. The missing ingredient is the relation of the mass flux to the water content at the position of the front, which is well known to be controlled by the pore size distribution of the porous material [13,38]. As follows from Figure 7 (see also Figure A1), the transition from stage 1 to stage 2 of evaporation was observed around the water content (less than the average of) $\sim$0.07, later during stage 2 decreasing quickly to $\sim$0.04 and even lower values ($\sim$0.02 for Sample 3) near the evaporation front. According to the pore size distribution measured using MIP (see Figure 3), the water content 0.07 corresponds to the pores smaller than 18 µm in radius; according to the functional PSD approximation using ANA (see Table 1), the same value corresponds to capillaries of the radius smaller than some value in the range 19.3–26.8 µm (20.4 µm by linear interpolation). The water content 0.04 corresponds to the pores smaller than the radius of 13 µm according to MIP, and functional capillaries smaller than 13.9 µm in radius according to the ANA method. Note, however, that the latter value, despite being strikingly consistent with MIP, is of considerable uncertainty, since the ANA results are based on comparing saturated fluxes through the capillaries, and the value corresponds to less than 0.2% of the total saturated flux for water (see Table 1).

Let us mention that the water content observed near the evaporation front and the corresponding pore sizes discussed above confirm that the vapor pressure near the evaporation front is not lowered due to the suction pressure in the evaporated menisci. According to Kelvin (or Ostwald–Freundlich) equation ([39]; Equations (3.23) and (3.33)), a relative vapor pressure lowering of no more than 0.1% corresponds to the water–vapor interface curvature of 1 µm radius. Since capillaries of size around 10 µm remain saturated at the evaporation front, the corresponding decrease in vapor pressure is certainly negligible.

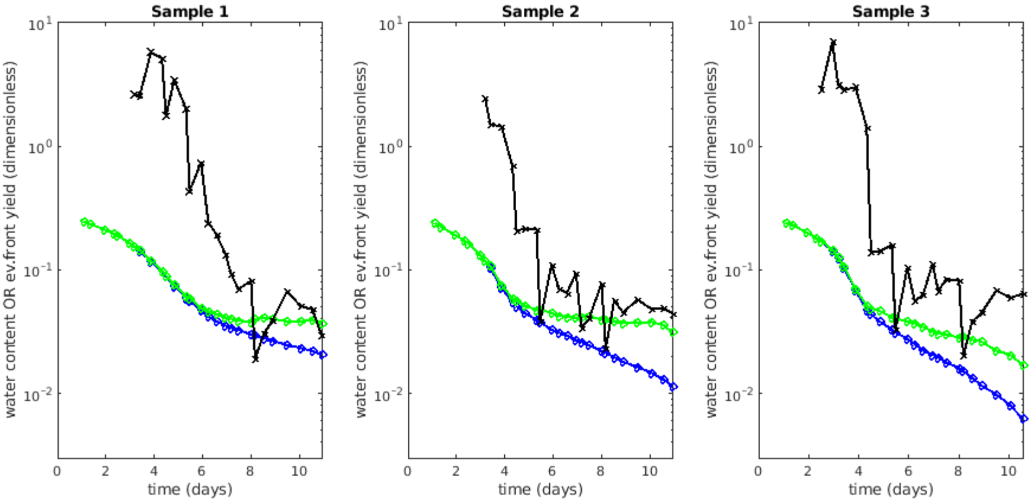

Figure 7. Evolution of average volumetric water content in the sample (blue) and in the capillary zone alone (green), "evaporation front yield" defined by evaporation rate divided by the evaporation front depth velocity (black). Note the logarithmic scale of the vertical axis.

4.3. Accuracy of Calculations

We consider the observed relative error of the calculated compared to measured evaporation rate of about 15% to be a relatively good and acceptable result, given the wide range of evaporation rates observed during the experiment, spanning more than one order of magnitude (0.1–3.5 mm/day). The Pearson correlation coefficient between measurements and calculations was >0.95 for individual samples, which is comparable to the findings in previous rock evaporation studies (average correlations of 0.81 and 0.91 in [18,19]. It is important to note that in the experiments presented, the evaporation front dynamically (and freely) moved, mimicking natural conditions and processes in rock outcrops. This is in contrast to previous studies where the evaporation front was carefully maintained at a specific depth below the rock surface.

For stage 2, the calculated values exhibited a high degree of agreement with the measurements, with the Pearson correlation coefficient of 0.98. For stage 1, the Pearson correlation coefficient was 0.42. The lower correlation observed is attributed to the fact that the measured evaporation rate exhibited a much greater degree of variability than the calculated one (see Figures 5 and 8). This demonstrates that the evaporation rate in stage 1 is influenced by other factors than the difference in partial pressures alone.

In stage 1, the other factor that determines the accuracy of the calculated evaporation rate is the parameter β. In the calculations presented so far, we used a value of β equal to 1.38 mm derived using the least squares method directly from the observed data. In the previous evaporation study by the author [18] that was performed on the JE sandstone in outdoor conditions in humid climate, the parameter β was determined to be equal 0.80 mm. When we apply $\beta = 0.80$ mm to our data, the difference between calculations and measurements increases from 0.21 to 1.6 mm/day, and the relative error increases from 9 to 72% (Table 2, Figure 8).

This reflects the fact that the parameter β is not solely determined by the properties of the porous material but is also influenced by the surrounding environment during evaporation. The value of 0.80 mm, which was associated with outdoor conditions, likely encompasses additional factors such as increased wind flow and solar radiation, which are absent or less pronounced in the present indoor settings. Consequently, when using a parameter $\beta = 0.80$ mm, the prediction strongly overestimates the evaporation rates under indoor conditions.

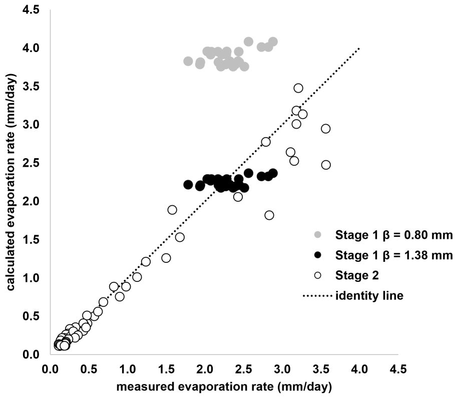

Figure 8. Goodness of fit between measured and calculated evaporation rate for Stage 1 (full circles, two distinct values of parameter β are used) and Stage 2 (open circles).

Among the available methods for measuring the depth of the evaporation front, the uranine-probe method stands out as the simplest, least expensive, and most accurate for field application. According to [22], the reported accuracy of this method is at least 2 mm. Since the evaporation rate is inversely proportional to the evaporation front depth L (for $L > \beta$), both the relative and absolute error in evaporation rate prediction due to the error in the measured front depth decreases significantly with increasing L. Assuming that the correct value L is not more than 2 mm distant from the measured value $L = L_m$, the mass flux j_m derived from the measured L_m has a relative error ε with respect to the correct flux j at most:

$$\varepsilon = \frac{|j - j_m|}{j} = \frac{2}{L_m}.$$

Note that the prediction of the correct flux j based on the measured value is not symmetric: knowing j_m, the correct flux j should be in the interval

$$j \in \left(\frac{1}{1+\varepsilon}, \frac{1}{1-\varepsilon} \right) j_m. \tag{7}$$

Overestimating the front depth therefore results in lower errors in the evaporation rate compared to underestimating. At a depth of 6 mm below the surface, the error given by 2 mm underestimation is reduced to 50%, and at 10 mm below the surface, the error decreases further to 25% (Figure 6B). Concerning the part of the three experiments when the evaporation front was no more than 6 mm below the sandstone surface in stage 2, the difference between the calculations and the measurements was 13% on average (0–44%) in our experiment. This corresponds to highly accurate measurements of the evaporation front depth (error 0.2–0.5 mm on average). Therefore, it seems that the real inaccuracy of the evaporation front depth measurements is lower than 2 mm in the laboratory practice. We further note that the primary source of inaccuracy arises from the capillary rise of moisture on the probe toward the surface, particularly when the tested sandstone is close to full saturation [22]. In the natural sandstone massif, especially in arid areas, typical moisture contents are far from full saturation [7,40] which also corresponds to higher depths of the evaporation front. For both of these reasons, a small error in the calculated evaporation rate can be anticipated.

4.4. Determining the Evaporation Rate from Natural Sandstone Outcrops

Our findings, together with previous studies, provide clear evidence that the position of the evaporation front plays a crucial role in the evaporation rate, potentially leading to variations of several orders of magnitude. The controlled indoor experiment simulates well the behavior and processes occurring in a natural sandstone massif. This is particularly applicable for situations where the evaporation front gradually recedes deeper below the surface due to none or insufficient water supply from the deeper subsurface. However, we see no obstacles in applying the findings also for scenarios where the subsurface flow is equal to the evaporation rate and the evaporation front remains stationary, or it slightly exceeds the evaporation rate and the evaporation front approaches the surface.

The dynamic evolution of the position of the evaporation front allows the outcome of the indoor experiment to be extrapolated to field conditions. While uncertainties related to the diffusion layer effect (parameter β) and inaccuracies in measuring the evaporation front depth may introduce some degree of error in calculating the evaporation rates from natural rock surfaces, the following should be considered.

The measured depth of the evaporation front represents only a localized point on the rock outcrop, and it is important to acknowledge the inherent variability within this small-scale observation. Surface irregularities in microrelief can lead to significant variations in the depth of the evaporation front over short distances, as much as centimeters over distances of several centimeters [7,22]. Furthermore, the thickness of the diffusion layer above the rock surface is likely to vary considerably over small areas, ranging from millimeters to centimeters, due to surface protrusions that create variations in water-vapor distribution and concentration gradients [41,42]. Therefore, in one place, evaporation may be limited by a dry surface layer that extends several centimeters deep, as the evaporation front recedes. However, in another nearby place, evaporation may be limited by a diffusion layer, where the evaporation front is directly at the surface. These combined effects can result in significant spatial variations in the evaporation rate.

Temporal variability is another important aspect to be considered. Previous field measurements [22,43] have revealed that the evaporation front's position can fluctuate up to 40 mm per month at the same point on the rock outcrop. This variability corresponds to changes in the evaporation rate of up to ∼1.5 orders of magnitude per month (!) for a shallow-positioned evaporation front, regardless of atmospheric conditions. Furthermore, the impact of the diffusion layer is expected to undergo changes over time due to varying climatic conditions such as wind [42] or solar radiation, which further influence the evaporation rate during stage 1.

Considering the spatial and temporal variability described above, errors resulting from inaccuracies in determining the depth of the evaporation front are overshadowed. Currently, accurately predicting the dynamics of both the evaporation front depth and the diffusion layer thickness in the field remains a challenge.

For stage 1, we propose to use the parameter β derived from previous long-term field studies. In [19], recommended values for ten different lithologies are provided, falling within a range of 1.9 ± 1.4 mm. It is important to note that evaporation is constrained by the available heat and cannot exceed the potential evaporation. Therefore, the calculated evaporation rates for stage 1 should always be compared with the estimates of potential evaporation at the place (e.g., obtained from the method of [44]) and the lower value of the two should be utilized.

In contrast, the second stage of evaporation does not involve the parameter β and very reliable values of the evaporation rate are obtained from the Fick's law as soon as the evaporation front depth L is known, the only additional parameters required being the difference in water-vapor partial pressure and the water-vapor diffusion coefficient of the rock. It is worth noting that in hot arid and semi-arid regions, where salt weathering is particularly pronounced [45], the position of the evaporation front can be expected mostly below the surface (i.e., stage 2; Supplementary Data in [19,22]), making stage 1 occurrences rather rare and the presented method a very powerful tool in such regions.

Another important consideration is the presence of hygroscopic salts in the pore water, which limit the maximum water content in the air and establish an equilibrium relative humidity in the pore space [46]. Consequently, the RH on the evaporation front may be less than 100% [47], resulting in a reduced gradient of water-vapor partial pressure and consequently a lower evaporation rate. Under specific conditions, particularly during wet periods when the RH at the sandstone surface is higher than the salt-controlled RH in the rock massif, the direction of the diffusive flux can even be reversed, leading to moisture absorption rather than evaporation. To enhance the accuracy of the calculated evaporation rate, it is therefore beneficial to employ the equilibrium relative humidity value, specific to the salt or salt mixture present, rather than assuming a RH of 100% on the evaporation front. This approach aligns with a recent study [20], where the value of RH of 75% was used for the evaporation rate calculations due to the presence of a halite solution. The combined effect of vapor pressure lowering due to capillary suction in the presence of salts should be investigated further ([48]).

4.5. Workflow Diagram of Determining the Evaporation Rate from Sandstone Outcrops

In this section, we provide a detailed suggested procedure (Figure 9) for determining the evaporation rate from natural sandstone outcrops, utilizing the combination of Fick's law and the uranine-probe method.

(i) The initial step involves drilling a hole several millimeters wide and deep enough to capture the depth of the evaporation front. This could be a few centimeters in humid climates or even decimeters in arid regions. If significant salt accumulation in the massif is expected, it is advantageous to collect the drilled dust for subsequent salt content analysis—studies [47,49] can serve as an example. To determine the equilibrium relative humidity for given salts, ref. [50] can be consulted. Additionally, for the analysis of multi-salt mixtures, the ECOS/RUNSALT model (e.g., [51]), can be utilized.

(ii) The depth of the evaporation front L is then measured within the pre-drilled hole using the uranine-probe method (for procedure details beyond the scope of this paper, see [22]). The frequency of measurement depends on the purpose of the research; for routine measurements we recommend a minimum frequency of one month, if no sudden increase of water content is anticipated. However, it is important to keep in mind that even a short period of time of the evaporation being close to the surface may account for a major amount of evaporation.

(iii) At the study site, RH and T measuring devices, such as Voltcraft or iButton, should be positioned. Based on our experience, it is advisable to place the device in a drilled hole, with the measuring part facing outwards and aligned with the rock surface, ensuring it is protected against rain. Recording every 60 min seems to be sufficient [18].

(iv) The water-vapor diffusion coefficient δ must be known for the evaporation rate calculation. It can either be measured directly for the particular rock being studied (see Section 2.1) or obtained from existing literature. Values from 8.1×10^{-12} to 3.2×10^{-11} s can be expected for sandstones [18,52] and values from 2.7×10^{-12} to 2.1×10^{-11} s have been measured for several other lithologies including igneous and metamorphic rocks (see [19]).

(v) The evaporation rate is then computed using (6), using the water-vapor diffusion coefficient, the ambient partial water-vapor pressure determined from the RH and T records using (3), and the measured evaporation front depth. For the case that the evaporation front is at the surface or close to the surface, the parameter β is required in (6). Recommended values for the parameter β for 10 lithologies are provided in [19], along with the procedure for determining the parameter β directly from measurements. If the evaporation front is at the surface, it is recommended to verify that the calculated values do not surpass potential evaporation. See [44] for a straightforward technique to do so, necessitating only air temperature measurement.

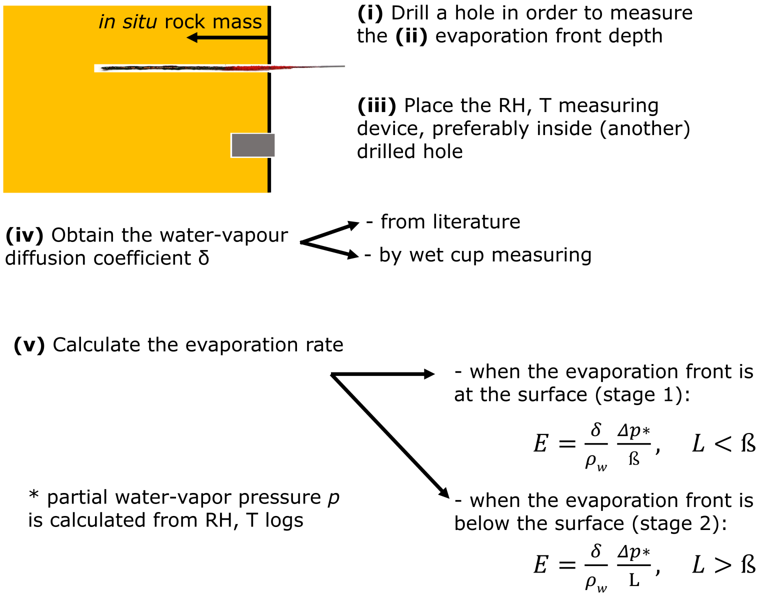

Figure 9. Workflow diagram of how to obtain the evaporation rate from natural sandstone outcrops.

4.6. Implications for Sandstone Weathering Research

By addressing the absent parameter in the water balance of natural rock outcrops—which was the evaporation rate—we acquire the capability to anticipate moisture content and its variations within the outcrops. This is particularly important for moisture-related sandstone weathering processes, including hydric and hygric weathering [53,54] and frost weathering, which is known to increase in efficiency with increasing moisture content [1,55].

As the rate of evaporation affects the quantity of accumulated salts [4], the calculation allows the determination of the relative rate of weathering and the identification of preferred weathering sites in the outcrops. Considering that the salt accumulates most at the evaporation front [5] and subflorescence is more destructive compared to efflorescence [56], the uranine-probe alone serves a straightforward yet potent benchmark for assessing the place and intensity of salt weathering.

The versatility of the method extends beyond geomorphology and allows for its application in cultural heritage studies. It can be utilized to identify areas of preferential weathering on statues, historical buildings, and other monuments, providing valuable insights into the preservation and conservation of these cultural treasures.

4.7. Suggested Future Research

The presented calculations of evaporation rate for the experiment in the indoor environment consider RH and T as the only climatic factors. In the outdoor conditions, including authentic ruiniform relief microclimates, previous studies on rock evaporation showed the accuracy of the estimates based only on RH and T [18,19], comparable to our findings. The close agreement between the calculated and measured values suggests that RH and T are the primary climatic factors influencing the evaporation rate, particularly in stage 2. This is further supported by [19], who demonstrated that realistic combinations of RH and T solely can lead to evaporation rate differences of up to an order of magnitude across various climatic zones.

On the other hand, studies on loose materials show that wind can increase evaporation rates by up to tens of percent under specific conditions [12,57,58]. Conversely, it has been reported [59] that fast wind may decrease evaporation rates by pushing the evaporation front deeper below the surface. It is important to accurately quantify the influence of other climatic factors in future studies and determine whether they should be included in order to enhance the evaporation rate estimate or whether they can be disregarded, considering the increased demands on field data collection. Another factor not considered in the present study, but worthy of future investigation, is the transport of water vapor in response to cyclic changes in atmospheric pressure, referred to as barometric pumping, which may enhance evaporation rates [60].

In the present study, the measurements were conducted on a single type of material, deliberately selected for its relatively high homogeneity in order to simplify the analysis. To the best of our knowledge, the evaporation from different rock types has only been studied in detail by [19], indicating that the discrepancy between calculated and measured evaporation rate increases with materials' heterogeneity. However, further investigation is required before drawing any quantitative conclusions.

Furthermore, it would be valuable to examine the impact of fractures and their morphology on the evaporation process from rock, as this area has not yet been thoroughly investigated. Based on analogous studies with loose materials [61], it can be expected that the presence of cracks may enhance evaporation rate. Additionally, it would be important to explore how increased material permeability to water vapor and the resulting increased evaporation rate due to cracks influence the spatial distribution of the evaporation front within the rock.

5. Conclusions

Under controlled laboratory conditions, we examined the evaporation process from sandstone samples during natural drying from complete saturation to residual moisture. Throughout the experiment, we analyzed the spatial distribution of moisture in the sandstone using the uranine-probe method, which measures the depth of the evaporation front underneath the surface, and we measured the evaporation rate from the samples. The measured values of the rate of evaporation were compared to values calculated from the measured evaporation front depth, based on Fick's law. To the best of our knowledge, this is the first time that Fick's law has been used to calculate the evaporation rate from a rock with a dynamically changing depth of the evaporation front, and the calculated values were compared to direct measurements.

As expected, we observed relatively constant high evaporation rates as long as the evaporation front remained at the surface (stage 1), and a rapidly decreasing evaporation rate once the front fell below the surface (stage 2). The measured values confirmed not only the inverse proportionality of the evaporation rate with the evaporation front depth during stage 2, consistent with the Ficks's law for water-vapor diffusion through the dry surface layer of the rock. More importantly, the measured evaporation rates were consistent with the prediction based on Fick's law, using the water-vapor diffusion coefficient measured independently of the evaporation experiment.

The calculated evaporation rate was in a good agreement with measurements over various depths of the evaporation front below the surface (with the Pearson correlation coefficient 0.98 and relative error of the calculations averaging 15%). For the case where the evaporation front was at the surface, the prediction model required knowledge of an additional parameter β, which characterises a thin diffusion layer of air above the surface.

The study clearly demonstrated the significant role of the depth of the evaporation front in evaporation from sandstone. The findings' transferability to field conditions is also discussed. The conclusions presented underscore the importance of measuring the depth of the evaporation front to determine in-situ evaporation rates from natural sandstone surfaces. The results have relevant implications for geomorphological investigations, particularly those pertaining to the impact of moisture-related weathering, encompassing salt and frost weathering, as well as bioweathering.

Supplementary Materials: The following supporting information can be downloaded at: https://www.mdpi.com/article/10.3390/hydrology11090133/s1, spreadsheet with measured data.

Author Contributions: M.S. conceieved and designed the study, contributed to the funding acquisition, performed the experiments, analysed and interpreted the data and prepared the original draft of the manuscript. M.L. contributed to funding acquisition, interpretation of the results, software development, data analysis and the review and editing of the manuscript. All authors have read and agreed to the published version of the manuscript.

Funding: This work was funded by the Czech Science Foundation, project number GA21-27291S.

Data Availability Statement: Data is contained within the article or Supplementary Material.

Conflicts of Interest: The authors declare no conflicts of interest.

Abbreviations

The following abbreviations are used in this manuscript:

RH	Relative Humidity
PSD	Pore Size Distribution
MIP	Mercury Intrusion Porosimetry
ANA	method by Abou Najm & Atallah

Appendix A. Porosimetry of the Sandstone Sample

In addition to MIP, we determined the approximated functional pore size distribution of the rock core using the method introduced by Abou Najm and Atallah ([30], here referred to as the ANA method). Assuming that saturated flow through a porous medium can be represented equivalently by flow through bundles of cylindrical capillaries, the functional pore size distribution is defined by the partial flux of water through capillaries of given size. The ANA method requires N values of volumetric flux measured for water and different non-Newtonian (shear-thinning) fluids. In this study, $N = 8$ with seven solutions of different concentrations of xanthan gum in distilled water. The shear-thinning viscosity η of each fluid was measured using a rotational viscometer (Anton Paar ViscoQC 300 L, for shear rates $\dot{\gamma}$ in the range ∼1.3–300 s) and characterized by the parameters μ and n of the power-law model

$$\eta = \mu\dot{\gamma}^{n-1}, \tag{A1}$$

as summarised in Table A1. The flux measurements were performed on a sample of JE sandstone, which was first saturated with deionised degassed water under 95% vacuum. The volumetric flux values listed in Table A1 were measured under the constant hydraulic gradient of 3 for water and for all seven xanthan gum solutions.

Table A1. Saturated flow experiments with aqueous xanthan gum solutions.

c (g/L)	μ (mPas^n)	n (–)	v (m/s) for $I = 3$
0 (water)	1.00	1	2.35×10^{-4}
0.3	10.7	0.705	5.03×10^{-5}
0.5	26.7	0.602	2.90×10^{-5}
0.7	106	0.442	5.92×10^{-6}
0.9	166	0.417	2.25×10^{-6}
1.1	158	0.412	8.88×10^{-7}
1.3	324	0.337	1.32×10^{-7}
1.7	616	0.272	1.76×10^{-8}

We then implemented the numerical inverse problem discussed in detail in [30] as “Problem Type 1”, which can be briefly summarized as follows. Each total flux v_i for the i-th fluid, is assumed to be the sum

$$v_i = \sum_{j=1}^{M} q_i(R_j)w_j, \tag{A2}$$

where the relative flux factors $q_i(R)$ are defined based on the Hagen–Poiseuille flow of i-th (power law) fluid through the cylindrical capillary of radius R, considering the known hydraulic gradient ($I = 3$) and the fixed tortuosity value 2, see the reference for more details. The flux factors are defined such that (A2) reads $1 = w_1 + \ldots + w_M$ for water. For $M = N = 8$ we prescribed the eight discrete representative radii R_j as the geometric sequence with endpoints 10 and 100 µm. The range of discrete radii was chosen by trial-and-error such that the computed weights (see in what follows) are positive but small at the endpoints. For given radii, the eight weights w_j (the relative fluxes for water) are determined by solving the constrained least squares problem of fitting the measured volumetric flux data v_i by (A2), subject to two additional constraints: (i) that all weights are positive and (ii) that the porosity defined by the functional capillaries equals the measured porosity value of 0.283, see the reference for details. The resulting functional PSD approximation is presented in Table 1 and Figure 3b.

Appendix B. Evaporation Rate, "Evaporation Front Yield", Average Water Content

We compare the measured evaporation rate and the "evaporation front yield" with the average water content in the wet capillary zone, see Figure A1. Note that during most of stage 2, the average water content values were in the range 0.04–0.07 and that during the same period the "yield" values were well above the average water content values. Moreover, both relations travelled quite consistently along the same path for the three measured samples, up to the moment when the "yield" reached the water content values and the three samples' behavior diverged, most likely due to their different heights and the correspondingly different remaining volume of the wet capillary zone.

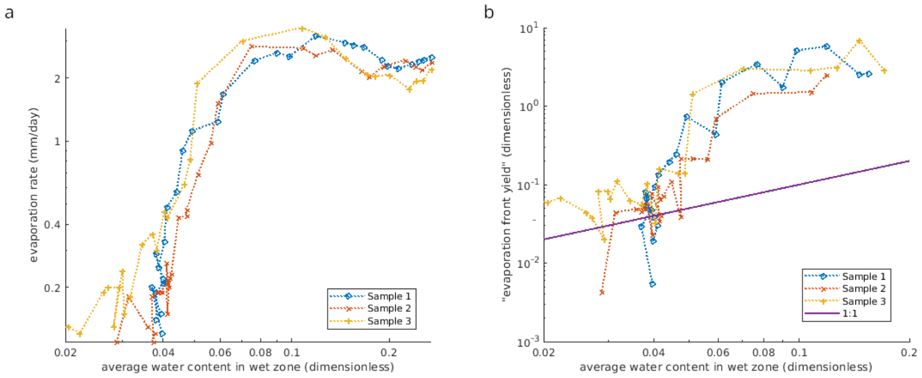

Figure A1. (**a**) Evaporation rate; or (**b**) "evaporation front yield" values compared to the average water content in the capillary zone. Note the logarithmic scale of all axes.

References

1. Hall, K. A Laboratory Simulation of Rock Breakdown Due to Freeze Thaw in a Maritime Antarctic Environment. *Earth Surf. Process. Landforms* **1988**, *13*, 369–382. [CrossRef]
2. Nicholson, D.T.; Nicholson, F.H. Physical deterioration of sedimentary rocks subjected to experimental freeze-thaw weathering. *Earth Surf. Process. Landforms* **2000**, *25*, 1295–1307. [CrossRef]
3. Richards, J.; Guo, Q.; Viles, H.; Wang, Y.; Zhang, B.; Zhang, H. Moisture content and material density affects severity of frost damage in earthen heritage. *Sci. Total Environ.* **2022**, *819*, 153047. [CrossRef] [PubMed]
4. Ruedrich, J.; Siegesmund, S. Salt and ice crystallisation in porous sandstones. *Environ. Geol.* **2007**, *52*, 343–367. [CrossRef]
5. Huinink, H.P.; Pel, L.; Kopinga, K. Simulating the growth of tafoni. *Earth Surf. Process. Landforms* **2004**, *29*, 1225–1233. [CrossRef]
6. Flatt, R.J. Salt damage in porous materials: How high supersaturations are generated. *J. Cryst. Growth* **2002**, *242*, 435–454. [CrossRef]
7. Bruthans, J.; Filippi, M.; Slavik, M.; Svobodova, E. Origin of honeycombs: Testing the hydraulic and case hardening hypotheses. *Geomorphology* **2018**, *303*, 68–83. [CrossRef]
8. Rodrigues, J.D. Swelling behaviour of stones and its interest in conservation. An appraisal. *Mater. Construcción* **2001**, *51*, 183–195. [CrossRef]
9. Wedekind, W.; Lopéz-Doncel, R.; Dohrmann, R.; Kocher, M.; Siegesmund, S. Weathering of volcanic tuff rocks caused by moisture expansion. *Environ. Earth Sci.* **2013**, *69*, 1203–1224. [CrossRef]

10. Or, D.; Lehmann, P.; Shahraeeni, E.; Shokri, N. Advances in Soil Evaporation Physics—A Review. *Vadose Zone J.* **2013**, *12*, 1–16. [CrossRef]
11. Shokri, N.; Lehmann, P.; Or, D. Liquid-phase continuity and solute concentration dynamics during evaporation from porous media: Pore-scale processes near vaporization surface. *Phys. Rev. E* **2010**, *81*, 046308. [CrossRef] [PubMed]
12. Haghighi, E.; Gianotti, D.J.S.; Akbar, R.; Salvucci, G.D.; Entekhabi, D. Soil and Atmospheric Controls on the Land Surface Energy Balance: A Generalized Framework for Distinguishing Moisture-Limited and Energy-Limited Evaporation Regimes. *Water Resour. Res.* **2018**, *54*, 1831–1851. [CrossRef]
13. Lehmann, P.; Assouline, S.; Or, D. Characteristic lengths affecting evaporative drying of porous media. *Phys. Rev. E* **2008**, *77*, 056309. [CrossRef] [PubMed]
14. Hall, C.; Hoff, W.; Nixon, M. Water-Movement in Porous Building-Materials VI. Evaporation and Drying in Brick and Block Materials. *Build. Environ.* **1984**, *19*, 13–20. [CrossRef]
15. Hall, C.; Hoff, W.D. *Water Transport in Brick, Stone and Concrete*, 2nd ed.; CRC Press: Boca Raton, FL, USA, 2013. [CrossRef]
16. McAllister, D.; Warke, P.; McCabe, S.; Gomez-Heras, M. Evaporative moisture loss from heterogeneous stone: Material-environment interactions during drying. *Geomorphology* **2016**, *273*, 308–322. [CrossRef]
17. Weiss, T.; Sass, O. The challenge of measuring rock moisture-a laboratory experiment using eight types of sensors. *Geomorphology* **2022**, *416*, 108430. [CrossRef]
18. Slavík, M.; Bruthans, J.; Weiss, T.; Schweigstillová, J. Measurements and calculations of seasonal evaporation rate from bare sandstone surfaces: Implications for rock weathering. *Earth Surf. Process. Landforms* **2020**, *45*, 2965–2981. [CrossRef]
19. Slavík, M.; Bruthans, J.; Schweigstillová, J. Evaporation rate from surfaces of various granular rocks: Comparison of measured and calculated values. *Sci. Total Environ.* **2023**, *856*, 159114. [CrossRef]
20. Mareš, J.; Bruthans, J.; Weiss, T.; Filippi, M. Coastal honeycombs (Tuscany, Italy): Moisture distribution, evaporation rate, tensile strength, and origin. *Earth Surf. Process. Landforms* **2022**, *47*, 1653–1667. [CrossRef]
21. Weiss, T.; Slavík, M.; Bruthans, J. Use of sodium fluorescein dye to visualize the vaporization plane within porous media. *J. Hydrol.* **2018**, *565*, 331–340. [CrossRef]
22. Weiss, T.; Mareš, J.; Slavík, M.; Bruthans, J. A microdestructive method using dye-coated-probe to visualize capillary, diffusion and evaporation zones in porous materials. *Sci. Total Environ.* **2020**, *704*, 135339. [CrossRef] [PubMed]
23. Mls, J. Evaporation front and its motion. *Hydrol. Earth Syst. Sci.* **2022**, *26*, 397–406. [CrossRef]
24. Richards, L.A. Capillary conduction of liquids through porous mediums. *Physics* **1931**, *1*, 318–333. [CrossRef]
25. Mareš, J.; Weiss, T.; Wieler, N.; Shtober-Zisu, N. Climate controls on limestone cavernous weathering patterns in Israel. *Geomorphology* **2024**, *462*, 109334. [CrossRef]
26. Mareš, J.; Bruthans, J.; Studencová, A.; Filippi, M. Moisture patterns and fluxes in evolving tafoni developed in arkosic sandstone in temperate climate. *Earth Surf. Process. Landforms* **2024** [CrossRef]
27. Fick, A. Ueber Diffusion. *Ann. Der Phys.* **1855**, *170*, 59–86. [CrossRef]
28. Czech Geological Survey. Geological map 1:50,000. Available online: https://mapy.geology.cz/geo/ (accessed on 19 August 2024).
29. Washburn, E.W. The Dynamics of Capillary Flow. *Phys. Rev.* **1921**, *17*, 273–283. [CrossRef]
30. Abou Najm, M.R.; Atallah, N.M. Non-Newtonian Fluids in Action: Revisiting Hydraulic Conductivity and Pore Size Distribution of Porous Media. *Vadose Zone J.* **2016**, *15*, vzj2015-06. [CrossRef]
31. Slavík, M.; Bruthans, J.; Filippi, M.; Schweigstillová, J.; Falteisek, L.; Řihošek, J. Biologically-initiated rock crust on sandstone: Mechanical and hydraulic properties and resistance to erosion. *Geomorphology* **2017**, *278*, 298–313. [CrossRef]
32. Tetens, O. Über einige meteorologische Begriffe. *Z. FüR Geophys.* **1930**, *6*, 297–309.
33. World Meteorological Organization. *Guide to Meteorological Instruments and Methods of Observation*; Number 8; World Meteorological Organization: Geneva, Switzerland, 2008.
34. Sultan, E.; Boudaoud, A.; Ben Amar, M. Evaporation of a thin film: Diffusion of the vapour and Marangoni instabilities. *J. Fluid Mech.* **2005**, *543*, 183–202. [CrossRef]
35. Wilson, G.W.; Fredlund, D.G.; Barbour, S.L. The effect of soil suction on evaporative fluxes from soil surfaces. *Can. Geotech. J.* **1997**, *34*, 145–155. [CrossRef]
36. Brutsaert, W.; Chen, D. Desorption and the 2 Stages of Drying of Natural Tallgrass Prairie. *Water Resour. Res.* **1995**, *31*, 1305–1313. [CrossRef]
37. Schultz, P. On the falling-rate period. *Chem. Eng. Technol.* **1991**, *14*, 234–239. [CrossRef]
38. Assouline, S. What Can We Learn From the Water Retention Characteristic of a Soil Regarding Its Hydrological and Agricultural Functions? Review and Analysis of Actual Knowledge. *Water Resour. Res.* **2021**, *57*, e2021WR031026. [CrossRef]
39. Lu, N.; Likos, W.J. *Unsaturated Soil Mechanics*; Wiley: Hoboken, NJ, USA, 2004.
40. Mol, L.; Viles, H.A. Geoelectric investigations into sandstone moisture regimes: Implications for rock weathering and the deterioration of San Rock Art in the Golden Gate Reserve, South Africa. *Geomorphology* **2010**, *118*, 280–287. [CrossRef]
41. Mosthaf, K.; Helmig, R.; Or, D. Modeling and analysis of evaporation processes from porous media on the REV scale. *Water Resour. Res.* **2014**, *50*, 1059–1079. [CrossRef]
42. Gao, B.; Farnsworth, J.; Smits, K.M. Evaporation from undulating soil surfaces under turbulent airflow through numerical and experimental approaches. *Vadose Zone J.* **2020**, *19*, e20038. [CrossRef]

43. Slavík, M. Moisture Characteristics of Natural Sandstone Exposures. Ph.D. Thesis, Charles University, Prague, Czech Republic, 2019.
44. Oudin, L.; Hervieu, F.; Michel, C.; Perrin, C.; Andréassian, V.; Anctil, F.; Loumagne, C. Which potential evapotranspiration input for a lumped rainfall-runoff model?: Part 2—Towards a simple and efficient potential evapotranspiration model for rainfall-runoff modelling. *J. Hydrol.* **2005**, *303*, 290–306. [CrossRef]
45. Cooke, R.U. Salt weathering in deserts. *Proc. Geol. Assoc.* **1981**, *92*, 1–16. [CrossRef]
46. Lubelli, B.; van Hees, R.P.J.; Groot, C.J.W.P. The effect of environmental conditions on sodium chloride damage-A step in the development of an effective weathering test. *Stud. Conserv.* **2006**, *51*, 41–56. [CrossRef]
47. Wedekind, W.; Ruedrich, J. Salt-weathering, conservation techniques and strategies to protect the rock cut facades in Petra/Jordan. In *Proceedings of the Heritage, Weathering and Conservation*; Fort, R., DeBuergo, M.A., Gomez-Heras, M., Vazquez-Calvo, C., Eds.; Taylor & Francis Ltd.: Abingdon, UK, 2006; Volumes 1 and 2, pp. 261–268.
48. Battistelli, A.; Calore, C.; Pruess, K. The simulator TOUGH2/EWASG for modelling geothermal reservoirs with brines and non-condensible gas. *Geothermics* **1997**, *26*, 437–464. [CrossRef]
49. Karatas, T.; Bruthans, J.; Filippi, M.; Mazancova, A.; Weiss, T.; Mares, J. Depth distribution and chemistry of salts as factors controlling tafoni and honeycombs development. *Geomorphology* **2022**, *414*, 991840. [CrossRef]
50. O’Brien, F. The Control of Humidity by Saturated Salt Solutions. *J. Sci. Instrum. Phys. Ind.* **1948**, *25*, 73–76. [CrossRef]
51. Godts, S.; Steiger, M.; Orr, S.A.; Stahlbuhk, A.; Desarnaud, J.; De Clercq, H.; Cnudde, V.; De Kock, T. Modeling Salt Behavior with ECOS/RUNSALT: Terminology, Methodology, Limitations, and Solutions. *Heritage* **2022**, *5*, 3648–3663. [CrossRef]
52. Pavlík, Z.; Michálek, P.; Pavlíková, M.; Kopecká, I.; Maxová, I.; Černý, R. Water and salt transport and storage properties of Msene sandstone. *Constr. Build. Mater.* **2008**, *22*, 1736–1748. [CrossRef]
53. Jiménez-González, I.; Rodríguez-Navarro, C.; Scherer, G.W. Role of clay minerals in the physicomechanical deterioration of sandstone. *J. Geophys. Res. Earth Surf.* **2008**, *113*, F02021. [CrossRef]
54. Ruedrich, J.; Bartelsen, T.; Dohrmann, R.; Siegesmund, S. Moisture expansion as a deterioration factor for sandstone used in buildings. *Environ. Earth Sci.* **2011**, *63*, 1545–1564. [CrossRef]
55. Matsuoka, N.; Murton, J. Frost weathering: Recent advances and future directions. *Permafr. Periglac. Process.* **2008**, *19*, 195–210. [CrossRef]
56. Rodriguez-Navarro, C.; Doehne, E. Salt weathering: Influence of evaporation rate, supersaturation and crystallization pattern. *Earth Surf. Process. Landforms* **1999**, *24*, 191–209. [CrossRef]
57. Ishihara, Y.; Shimojima, E.; Harada, H. Water-Vapor Transfer Beneath Bare Soil Where Evaporation Is Influenced by a Turbulent Surface Wind. *J. Hydrol.* **1992**, *131*, 63–104. [CrossRef]
58. Pourbakhtiar, A.; Poulsen, T.G.; Wilkinson, S.; Bridge, J.W. Effect of wind turbulence on gas transport in porous media: experimental method and preliminary results. *Eur. J. Soil Sci.* **2017**, *68*, 48–56. [CrossRef]
59. Shahraeeni, E.; Lehmann, P.; Or, D. Coupling of evaporative fluxes from drying porous surfaces with air boundary layer: Characteristics of evaporation from discrete pores. *Water Resour. Res.* **2012**, *48*, W09525. [CrossRef]
60. Auer, L.H.; Rosenberg, N.D.; Birdsell, K.H.; Whitney, E.M. The effects of barometric pumping on contaminant transport. *J. Contam. Hydrol.* **1996**, *24*, 145–166. [CrossRef]
61. Poulsen, T.G. Predicting evaporation from moist, cracked soil, based on near-surface wind speed, crack width and crack distance. *Eur. J. Soil Sci.* **2022**, *73*, e13215. [CrossRef]